Applied Catalysis B: Environmental 142–143 (2013) 368–376

Contents lists available at SciVerse ScienceDirect

Applied Catalysis B: Environmental

journal homepage: www.elsevier.com/locate/apcatb

Catalytic upgrading of the light fraction of a simulated bio-oil over $CeZrO_x$ catalyst

Sikander H. Hakim[a], Brent H. Shanks[b,c], James A. Dumesic[a,*]

[a] Department of Chemical and Biological Engineering, University of Wisconsin, Madison, WI 53706, USA
[b] Department of Chemical and Biological Engineering, Iowa State University, Ames, IA 50011, USA
[c] Biorenewables Research Laboratory, Iowa State University, Ames, IA 50011, USA

ARTICLE INFO

Article history:
Received 15 February 2013
Received in revised form 3 May 2013
Accepted 10 May 2013
Available online 27 May 2013

Keywords:
Bio-oil
Acetic acid
Acetol
Furfural
Upgrading

ABSTRACT

We present a catalytic strategy to upgrade the light fraction of a simulated bio-oil, consisting of acetic acid, acetol, and furfural. The acid content of the feed was significantly reduced by ketonization at 623 K over a ceria–zirconia ($CeZrO_x$) mixed oxide catalyst. The presence of furfural decreased the ketonization activity; however, it was possible to regain the initial catalytic activity by removal of furfural from the feed. Acetol was highly reactive over the mixed oxide, and its presence did not influence the ketonization activity. The results from reaction kinetics measurements for conversion of acetol suggest that the primary products are pyruvaldehyde and 1,2-propylene glycol formed by transfer hydrogenation. These two primary products then undergo reactions in series and parallel to produce an array of C_3–C_6 carbonyl compounds, constituting an upgraded intermediate feed appropriate for further processing steps to obtain transportation fuel components.

1. Introduction

Diminishing fossil fuel reserves and increasing transportation fuel demand have focused recent attention to alternative sources of carbon for the production of liquid fuels. Utilization of biomass has emerged as an important option in this respect, because it is the only sustainable source of organic carbon, making biofuels the only sustainable source of liquid hydrocarbon fuels [1,2]. Fast pyrolysis is an important technology for biomass processing, mainly due to its low capital and operating costs, and bio-oil (also known as pyrolysis oil or bio-crude) is the least expensive liquid fuel that can be obtained from lignocellulosic biomass [3]. Unfortunately, bio-oil is a poor quality fuel, with almost half the energy density as compared to petroleum-derived fuels, due to the high extent of oxygen functionalities in the bio-oil components. Excess functionality also makes it difficult to control the reactivity of bio-oil and direct conversion to targeted compounds. Thus, there is a need for processes that lead to a reduction of the oxygen content of the molecules in bio-oil, leading to the production of less-reactive intermediates that can be further upgraded to the desired products [4]. Additionally, bio-oil contains a large amount of organic acids, which poses problems of corrosion. Also, the presence of acid can catalyze an array of reactions in bio-oil, thereby leading to instability of the bio-oil. Thus, converting the acid content is crucial for rendering stability to bio-oil.

The high reactivity of the oxygen functionalities in bio-oil can be positively utilized to achieve C—C bond forming reactions, such as ketonization and aldol condensation. This coupling is particularly attractive for smaller oxygenates, whereby the molecular weight of the species can be increased such that most of the carbon can be retained in the liquid product in the targeted fuel range. This coupling is not possible with conventional hydrotreating, where the light oxygenates would lead to the undesired production of light gases (e.g., C_2–C_3 species) [5]. The ketonization reaction, which involves coupling of two carboxylic acids to produce a ketone with $2n-1$ carbon atoms, CO_2 and H_2O, is especially attractive for bio-oil upgrading, because it not only decreases the acid content of bio-oil, but it also removes oxygen as CO_2. This reaction has been extensively examined in the synthesis of a variety of ketones [6–9]. It can be achieved over an array of single and mixed metal oxides catalysts [10,11], and it has been proposed for use in decreasing the acid content in bio-oil [6,12]. However, bio-oil consists of hundreds of compounds and it is thus necessary to perform the ketonization reaction in the presence of other bio-oil components. In the present study, we evaluate the feasibility of ketonization as a bio-oil upgrading strategy by performing a systematic study of simulated bio-oil feeds, based on the GC–MS identification of various components of bio-oils from the literature [13]. The simulated feed (Table 1) contained acetic acid as a representative molecule for the carboxylic acids present in the bio-oil, acetol

* Corresponding author. Tel.: +1 608 262 1095; fax: +1 608 262 5434.
E-mail address: dumesic@engr.wisc.edu (J.A. Dumesic).

0926-3373/$ – see front matter © 2013 Elsevier B.V. All rights reserved.
http://dx.doi.org/10.1016/j.apcatb.2013.05.021

Table 1
Composition of simulated bio-oil feed.

Component	wt%
Acetic Acid	20
Furfural	5
p-Cresol	10
Acetol	10
Levoglucosan	2
Water	53
	100

representing hydroxyaldehydes/hydroxyketones, furfural (furans and derivatives), *p*-cresol (phenolics), levoglucosan and water.

Ceria-based catalysts have proven to be effective for ketonization of oxygenates [7,11]. Hasan et al. performed FTIR investigations to compare the ketonization activity of CeO_2 with other oxides such as TiO_2 and Al_2O_3 and found that the conversion of acetic acid to acetone occurred on TiO_2 and CeO_2, but not on Al_2O_3 [14]. This behavior was attributed to the presence of reducible Lewis sites on both TiO_2 and CeO_2, which were not present on Al_2O_3. Ceria was found to be the most active catalyst and this higher activity of CeO_2 was suggested to be due to its more facile reduction. Using FTIR investigations, the authors suggested the catalytic centers to be Lewis acid–base pairs. Shanks et al. suggested that the underlying mechanism for the ketonization reaction involves carboxylate species [15]. Resasco et al. suggested that the role of reduced Lewis acid sites in ketonization reaction could be the stabilization of the surface carboxylate [16]. A surface with high density of Ce^{3+} reduced sites will thus allow the formation of carboxylate pairs necessary for C—C coupling. XPS studies have indicated an increase in the content of Ce^{3+} on the oxide surface in the presence of acid [7]. It has been shown that the reducibility of CeO_2 is further improved by forming solid solutions with other metal oxides such as ZrO_2 [17,18]. Additionally, the incorporation of a second oxide also offers improved stability to CeO_2 catalysts, which are otherwise known to deactivate at high temperatures. The insertion of ZrO_2 into the cubic CeO_2 resulted in distortion of the mixed oxide structure, and as a result the reduction is no longer confined to the surface but involved the bulk oxide as well [17,19]. For a series of catalysts with increasing ZrO_2 content, Gutiérrez-Ortiz et al. found, based on H_2 consumption, that the reducibility was highest for $Ce_{0.5}Zr_{0.5}O_2$, and this catalyst contained the highest percentage of Ce^{3+}. It was also pointed out that there was no contribution from the reduction of ZrO_2. Mallinson et al. reported condensation reactions (ketonization and aldol condensation) of propanal over $Ce_xZr_{1-x}O_2$ mixed oxides prepared with varying compositions and observed that ketonization reactions via propionates were significantly reduced for samples with higher ZrO_2 content [7]. This behavior could potentially be due to lower density of reducible Lewis acid sites–base sites pairs. However, for that material there was a significant increase in the yield of aldol condensation products from propanal, with maximum propanal conversion taking place over pure ZrO_2. This promotion of aldol reactions over amphoteric oxides such as ZrO_2 has been suggested to be due to the presence of a balance of weak Lewis acid sites (metal cations) and neighboring intermediate strength $M^{x+}\cdots O^{2-}$ basic site pairs which are efficient in promoting aldol condensation [20]. It was also suggested that strong basic sites associated with low coordination O^{2-} present lower condensation rates, because isolated O^{2-} hinders stabilization of anionic intermediates for aldol condensation. This effect also explains the lowest conversion of propanal over pure CeO_2 [7]. In that study, the composition of $Ce_{0.5}Zr_{0.5}O_2$ catalyst was found to be optimum for catalyzing both ketonization and aldol condensation reactions [7]. Thus, it appears that this composition of ceria-zirconia mixed oxide catalysts offers the best combination of ketonization activity (for converting the acid content in bio-oil), aldol condensation activity (for simultaneous upgrading of other light oxygenates) as well as catalyst stability. Additionally, we have previously reported that in the conversion of biomass-derived carbohydrates (glucose and sorbitol), a $CeZrO_x$ catalyst (with Ce to Zr molar ratio of 1) was efficient and robust for ketonization of carbohydrate-derived carboxylic acids in the presence of other mono-functional oxygenated species [6,21]. Based on these results, we carried out upgrading studies with a $CeZrO_x$ catalyst to evaluate its performance for the ketonization of acetic acid in the presence of other components in the simulated bio-oil. The work presented here discusses the influence of various components on the ketonization activity. Additionally, this work discusses reaction mechanisms and associated intermediates in the conversion of acetol over the mixed oxide catalyst. To the best of our knowledge, a detailed reaction mechanism for the conversion of acetol has not been reported in literature and is of relevance for future upgrading studies.

2. Experimental

2.1. Catalyst synthesis

The $CeZrO_x$ mixed oxide catalyst was prepared from nitrate precursors by co-precipitation, as described elsewhere [19]. In short, an aqueous solution of $Ce(NO_3)_3{\cdot}6H_2O$ (Aldrich, 99%) and $ZrO(NO_3)_2{\cdot}xH_2O$ (Aldrich, 99%) was prepared to obtain a Ce/Zr ratio of 1. The precursor solution was added to an alkaline solution of pH 10 adjusted using NH_4OH (Aldrich, 28–30% stock solution) to initiate the precipitation process. The resulting slurry was aged under stirring at room temperature for 72 h at pH 10. The solids were separated by filtration, washed with de-ionized water and ethanol, dried at 373 K overnight, and calcined in air at 723 K for 2 h, with a heating rate of 3 K min^{-1}.

2.2. Catalyst characterization

The micro/meso-structural properties of $CeZrO_x$ mixed oxide catalyst were evaluated using a Micromeritics ASAP-2020 analyzer. The specific surface area of the material was obtained from the nitrogen adsorption–desorption isotherm at liquid nitrogen temperature by using the Brunauer–Emmett–Teller (BET) approach. Pore size distribution and pore volume were calculated from the desorption branch using the Barret–Joyner–Halender (BJH) method.

Ammonia and carbon dioxide temperature programmed desorption (TPD) experiments were carried out to estimate the total number of acidic and basic sites on the catalyst surface. For desorption experiments, 0.5–1.0 g of catalyst was loaded into a fritted quartz reactor tube (0.5 in. outer diameter). The tube was heated to the desired temperature using a well-insulated furnace connected to a variable power supply and a PID temperature controller (Love Controls) with a K-type thermocouple (Omega). The gas effluent was monitored by a mass spectrometer system and recorded by Omnistar software. Prior to desorption experiments, the loaded catalyst was treated at 523 K under flowing helium (100 cm^3 (STP) min^{-1}) for 1 h and then cooled to the desorption temperature (423 K for NH_3 and 300 K for CO_2, respectively). Ammonia was adsorbed onto the catalyst by exposure to flowing 1 mol% NH_3 in helium (100 cm^3 (STP) min^{-1}) at 423 K for 30 min. Residual NH_3 was removed by purging the catalyst with helium (100 cm^3 (STP) min^{-1}) at 423 K for 1 h. Carbon dioxide adsorption was carried out in a similar manner as ammonia adsorption, except that the catalyst was exposed to 5 mol% CO_2 in nitrogen and both adsorption and purging steps were performed at 300 K. Desorption

of NH_3 and CO_2 was performed by heating the catalyst at a rate of 10 K min^{-1} under flowing helium (45 cm^3 (STP) min^{-1}) from purging temperature to 1073 K for NH_3 and 1123 K for CO_2.

The elemental composition of the $CeZrO_x$ mixed oxide catalyst was determined at Galbraith labs by inductively coupled plasma atomic emission spectrometry (ICP-AES) using an ICP-OES Optima 5300 analyzer. The instrument measures characteristic emission spectra by optical spectrometry. Samples for analysis were prepared by mixing an appropriate amount of lithium meta/tetra borate flux and fused at 1270 K in a platinum crucible. The resulting melt was dissolved in a dilute nitric acid quenching solution which was then brought to volume and used for analysis.

2.3. Flow reaction studies

All reaction feed solutions were prepared from high purity chemicals: acetic acid (Sigma–Aldrich, 99.7%), acetol (Aldrich, 90%), furfural (Aldrich, 99%), *p*-cresol (Fluka, 99%) and levoglucosan (Carbosynth, UK). All experiments were performed in a fixed-bed, down-flow reactor consisting of a half-inch stainless steel tube. The $CeZrO_x$ catalyst was mixed with crushed fused silica (Aldrich) to maintain the bed height. 1–4 g of catalyst was loaded for various runs. The bed was held in place by quartz wool (Grace, Discovery Sciences). The tube was heated to the reaction temperature of 623 K using aluminum blocks heated by a well-insulated furnace. The reactions were carried out at atmospheric pressure. The simulated bio-oil liquid feed was supplied to the reactor using HPLC pumps (SSI Series 1 HPLC pump) at a total liquid flow rate of 2.4 ml h^{-1}, and prior to entering the reactor, the feed was separated into light and heavy fractions using a separator maintained at a temperature of 403 K. Helium gas was used to sweep the light fraction vapors from the separator to the reactor through heated lines. Subsequent to the reactor, a gas–liquid separator at room temperature was installed to collect the liquid phase reaction effluent for analysis using HPLC (Waters e2695 equipped with 2414 RI detector), GC–MS (Shimadzu GC-2010 with a mass spectrometer and Rtx-5 column), and GC–FID (Shimadzu GC 2010 with an Agilent DB-5ms column) and the gas phase products for analysis using on-line GC–TCD (Shimadzu GC-2014 with a Alltech HayeSep® DB 100/120 column) and GC–FID (Agilent 6890 equipped with an FID and GS-Q column). Tetrahydropyran (THP) (Sigma–Aldrich, 99%) was used to separate the liquid product into organic and aqueous phases for analysis. The experimental setup designed for this study efficiently separates the components into light and heavy fraction prior to entering the reactor. The heavy ends were collected from the separator, to be processed later by other methods, and these species are not the focus of the present work.

3. Results

3.1. Catalyst characterization results

The textural properties of $CeZrO_x$ mixed oxide catalyst in terms of surface area, pore volume and pore size are presented in Table 2. The surface area of the material obtained after calcination at 723 K for 2 h was 138 m^2/g. This value is consistent with previous reports of the synthesized material [19]. The isotherm obtained was a type IV isotherm, consisting of an H2 hysteresis loop indicative of the presence of mesopores in the material [22]. The elemental analysis of the calcined material indicated a Ce:Zr ratio close to the initially added ratio of Zr 30 wt% and Ce 47 wt%.

The TPD profiles of NH_3 and CO_2 were integrated to obtain the quantity of total surface acid and base sites per gram of catalyst. The NH_3 desorption profile displayed a single uniform peak in the temperature range of 560–600 K, suggesting a narrow distribution of acid sites on the surface. These results are consistent with the findings of Gurbuz et al., where the authors studied a series of mixed oxides of varying ZrO_2 composition and suggested that surface acidity is associated primarily with ZrO_2 [23]. The CO_2 desorption profile, however, indicated the presence of base sites of varying CO_2 adsorption strength. The CO_2 profile can be divided into three regions representing weak adsorption sites (300–500 K), intermediate strength adsorption sites (500–700 K) and strong adsorption sites (700–1000 K) [20]. The total amount base sites was calculated to be 149 μmol/g, of which around 37% were weak, 36% were of intermediate strength and 26% of the total sites were strong base sites. It has been suggested that the weak CO_2 binding sites are associated with the formation of bicarbonates due to surface OH^-, the intermediate strength sites are associated the formation of bridged and bidentate carbonates on the $M^{x+}\cdots O^{2-}$ pairs, while the strong CO_2 binding sites are associated with the isolated low coordination O^{2-} ions and the formation of more strongly bound unidentate carbonates [23].

Using CO_2 TPD experiments, Gurbuz et al. observed for ceria–zirconia mixed oxide catalysts prepared with varying composition that pure ZrO_2 possess only weak and medium strength adsorption sites associated with OH^- and $M^{x+}\cdots O^{2-}$ pairs, respectively, whereas the mixed oxide possesses a mixture of weak, intermediate strength and strong sites [23]. As the ZrO_2 content increases, the number of strong CO_2 binding sites (low coordination O^{2-} ions) diminishes, indicating that the strong binding sites are associated only with ceria. It was also noted that the mixed oxide possess a greater number of intermediate strength binding sites than either pure CeO_2 or ZrO_2, likely arising from the surface heterogeneity introduced by substituting Ce^{4+} ions with Zr^{4+} ions. Thus, it can be inferred that the presence of ZrO_2 in $CeZrO_x$ increases the surface Lewis acid site density and increases the density of intermediate strength basic sites, while ZrO_2 decreases the density of strong basic sites that are found only on the surface of pure CeO_2. As discussed earlier, this shift in the acid base properties along with the enhanced reducibility of the mixed oxide is favorable for promoting both C—C coupling reactions, ketonization and aldol condensation.

3.2. Ketonization reaction of acetic acid

To understand the influence of individual bio-oil components on the ketonization of acetic acid, we conducted studies by gradually increasing the complexity of the feed, starting with a feed consisting of pure acetic acid feed (20 wt% in water) and eventually attaining the feed composition represented in Table 1. Scheme 1 represents the ketonization reaction where two acetic acid molecules condense to produce a molecule of acetone, CO_2 and H_2O.

Fig. 1 shows the catalytic performance of the $CeZrO_x$ catalyst for acetic acid ketonization performed at 543 K. All experiments, unless otherwise stated, were performed at atmospheric pressure and with a weight hourly space velocity (WHSV) of 0.6 h^{-1}. The catalyst demonstrated excellent stability for over 300 h on stream. These reaction conditions resulted in a steady state conversion of 50%, and around 90% of the theoretical selectivity was achieved for acetone and CO_2. No other products were detected in GC–FID/TCD/MS analysis of the reaction products.

3.3. Influence of furfural

Reaction kinetics studies were next performed by adding 10 wt% furfural to the feed. Under similar reaction conditions, furfural strongly inhibited the ketonization reaction, such that the conversion of acetic acid decreased to below 5% within 40 h on stream. Although furfural resulted in a strong inhibition of acetic acid ketonization, furfural did not undergo significant conversion

Table 2
Characterization results for $CeZrO_x$ mixed oxide catalyst calcined at 723 K for 2 h.

Catalyst	NH_3 (TPD) (μmol/g)	CO_2 (TPD) (μmol/g)	BET surface area (m^2/g)	BJH pore volume (cc/g)	Avg. BJH pore size (nm)	Ce (wt%)	Zr (wt%)
$CeZrO_x$	62	149	138	0.25	6.3	46.5	24.4

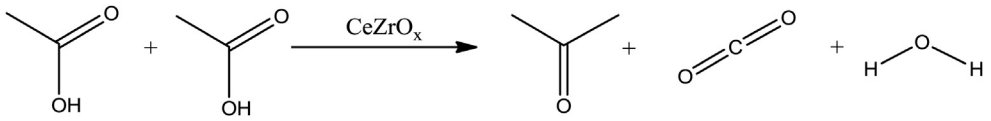

Scheme 1.

(5–10%). Thus, it appears that furfural blocks surface sites on the catalyst for the ketonization reaction. To investigate this hypothesis and to probe whether this coverage of active sites could be ameliorated at higher temperature, the ketonization reaction was carried out at 623 K. Under these conditions, we found that it was possible to achieve ketonization of acetic acid in the presence of furfural, during which 20% of the furfural underwent conversion to decarbonylation products, such as furan, methyl furan and, an aldol condensation product with acetone, 4-(2-furyl)-3-buten-2-one. This aldol condensation product with acetone has previously been observed by West et al. while performing C—C coupling studies with biomass-derived furfurals [24].

To further investigate the nature of deactivation caused by the presence of furfural, experiments was performed at 623 K where for the first 100 h on stream, the feed contained pure acetic acid (20 wt% in water), followed by introduction of furfural into the feed. As seen in Fig. 2, the presence of furfural resulted in the suppression of ketonization activity, such that the conversion of acetic acid decreased to 45% over next 100 h (Fig. 2). The figure also shows the conversion of furfural, from which can be seen that furfural was minimally converted by the end of the run. Next, the furfural was removed from the feed, after which the ketonization activity started to increase again, and the original conversion was regained at the end of the run. Thus, although the presence of furfural deactivates the catalyst, possibly by blocking active sites, this deactivation is reversible.

3.4. Reactions with full simulated feed

In the next step of the study, *p*-cresol (10 wt%) was added to the feed using two different HPLC pumps to supply organic and aqueous portions to arrive at the desired feed composition. The introduction of *p*-cresol into the feed resulted in reactor plugging due to solidified phenolic species at both ends of the reactor tube.

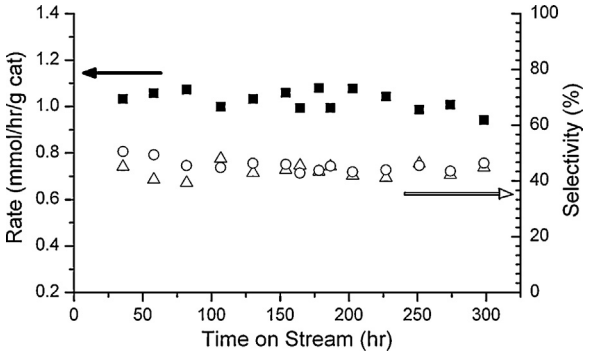

Fig. 1. Performance of $CeZrO_x$ catalyst versus time-on-stream for acetic acid ketonization at 543 K. Left vertical axis indicates the rate of acetic acid conversion (solid squares), and the right axis indicates carbon dioxide (open circles) and acetone (open triangles) selectivities (moles produced per mole of acetic acid converted).

We also carried out the reaction at a higher pressure of 300 psi to retain the lighter components in the liquid phase; however, operating at the higher pressure only slowed the reactor plugging process. A combination of higher pressure and lower amount of *p*-cresol (2 wt%) allowed the feed to be processed without reactor plugging. Subsequent reaction kinetics studies showed that the presence of *p*-cresol at this lower level did not cause significant deactivation of the catalyst, and similar deactivation profiles were obtained with and without *p*-cresol in the presence of furfural. In particular, the conversion of acetic acid decreased to around 49% after 60 h on stream. Most of the *p*-cresol was recovered in the liquid product stream with minimal conversion. This result with *p*-cresol is in agreement with the findings of Deng et al. [12].

In subsequent studies, we added 5 wt% acetol to the above feed containing acetic acid, furfural and *p*-cresol. Reaction kinetics measurements indicated that acetol did not cause a significant change in the deactivation profile. However, acetol is highly reactive under these conditions, undergoing 83% conversion. GC–MS analysis revealed that the new products formed from acetol included an array of C_3–C_6 carbonyl compounds. To further understand the influence of acetol, a feed was prepared with only acetic acid (20 wt%) and acetol (5 wt%). We found that both the components underwent more than 99% conversion. Thus, the presence of acetol does not influence the ketonization activity, but it is highly reactive over the mixed oxide catalyst.

The last component introduced into the feed was levoglucosan, which again led to reactor plugging due to thermal polymerization at the entry of the reactor tube [25,26]. This plugging was observed for even small quantities of levoglucosan (e.g., 0.5 wt%). Thus, for continuous operation of the flow reactor, it was found to be necessary to eliminate phenolics and levoglucosan from the feed. The strategy that was adopted for subsequent upgrading reactions

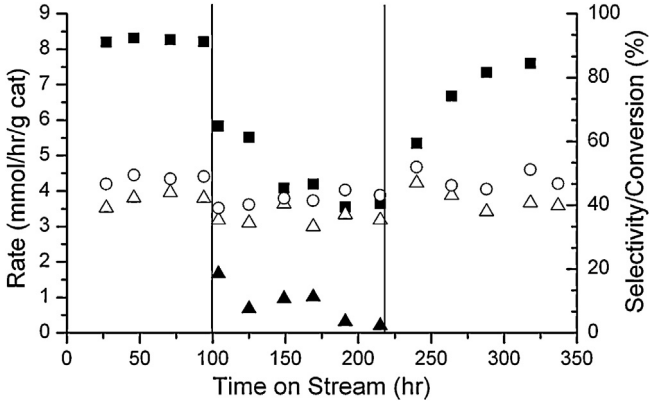

Fig. 2. Influence of addition of furfural on the ketonization activity of $CeZrO_x$. Left vertical axis indicates the rate of acetic acid conversion (solid squares), and the right axis indicates carbon dioxide (open circles) and acetone (open triangles) selectivities (moles produced per mole of acetic acid converted) and furfural conversion (solid triangles).

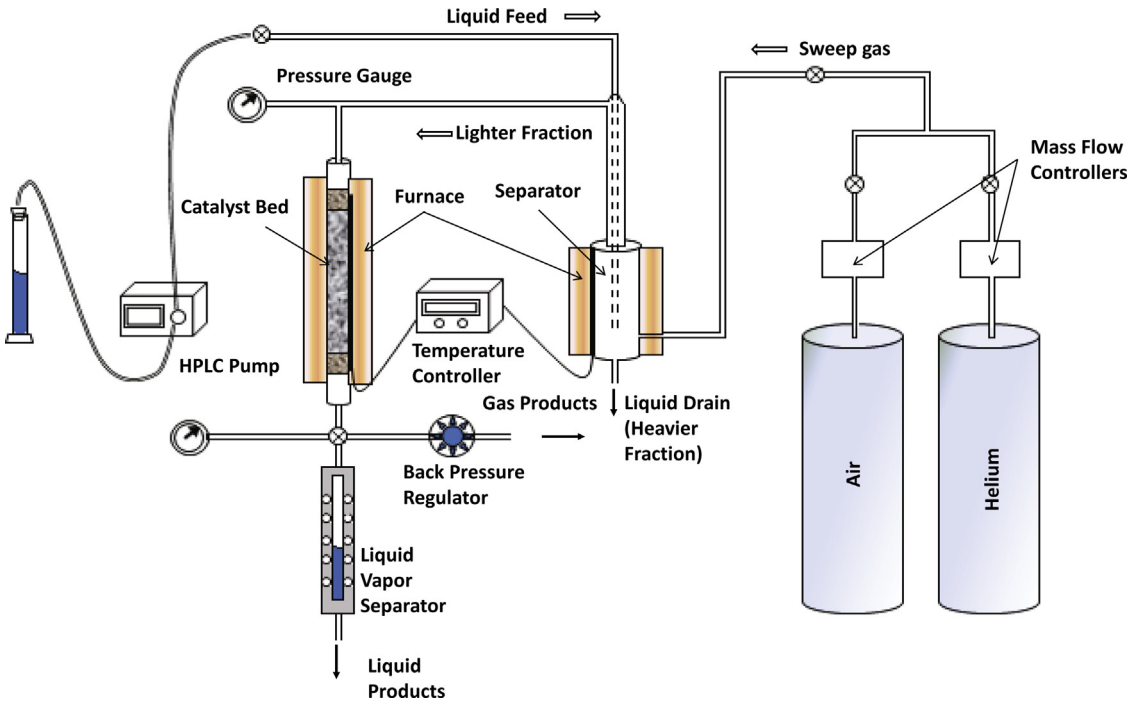

Fig. 3. Reactor setup used for upgrading of simulated bio-oil.

was to modify the reactor set-up to efficiently separate the light ends (acetic acid, furfural, acetol) from heavy ends (*p*-cresol, levoglucosan), such that the light ends could be processed through the catalyst bed, whereas the heavy ends were collected from a separator prior to entering the reactor.

3.5. Modification of the reactor system

The schematic representation of the reactor system modified to process feeds containing phenolics and levoglucosan is shown in Fig. 3. In this reactor set-up, a separator at 403 K was installed prior to the reactor. The feed was pumped into the separator, where an inert gas (helium) swept the vapors of light components to the reactor, whereas the heavy ends were collected at the bottom of the separator (Fig. 3). The gas and liquid products were collected and analyzed from the reactor outlet.

To evaluate the performance of this reactor set-up and to investigate thermal reactions that might be occurring, the feed was introduced to the reactor without any catalyst bed. Table 3 presents the reactant and product distribution, where about 90% of *p*-cresol and levoglucosan was recovered at the separator, while more than 90% of acetic acid, 70% of acetol and 80% of furfural was carried over to the reactor. With no catalyst, the components underwent minimal conversion with only some light gases detected as products.

The simulated bio-oil feed was then passed into the modified reactor system containing the $CeZrO_x$ catalyst bed. The distribution of reactants and product distribution is presented in Table 4.

In the presence of catalyst, after 40 h on stream, the conversions of acetic acid, acetol, and furfural were equal to 60%, 90%, and 29%, respectively. Acetone was the major product. The remaining carbon in the products was present in products from acetol (mainly C_3–C_6 carbonyls) and furfural (mainly furans, and 4-(2-furyl)-3-buten-2-one). All of the levoglucosan and more than 85% of the *p*-cresol were recollected at the separator. The total C balance was 87.4%. This heavy fraction collected from the separator can be set aside to be processed by other strategies. From this fraction, all of the levoglucosan could be extracted into the aqueous phase upon addition of water. The remaining organic phase, rich in phenolics could be upgraded by hydrodeoxygenation (HDO) reactions in the presence of hydrogen, a brief account of which is discussed below. However, upgrading of the heavy fraction is beyond the scope of current work.

Hydrodeoxygenation (HDO) is considered to be the most promising route for upgrading the phenolic component of bio-oil [27–29]. Because of their ring structures, these compounds can be converted to renewable gasoline additives by HDO to aromatics and cyclic aliphatic hydrocarbons [29,30]. For instance, *p*-cresol can be hydrodeoxygenated to produce toluene with a research octane number (RON) of 120 and methyl cyclohexane with a RON of 75 [31]. Conventional HDO catalysts developed for petroleum hydroprocessing such as sulfided CoMo, NiMo catalysts have been tested for upgrading of phenolics in bio-oil to produce transportation fuel grade components [32]. Although such catalysts are effective, their use for reductive upgrading of bio-oil entails several drawbacks, the main issues being product contamination by sulfur incorporation, catalyst deactivation by coking, and catalyst poisoning by the presence of water [33,34]. Supported noble metal catalysts such as Pt, Pd and Ru have also been tested [28]. Such catalyst systems are more attractive, because HDO reactions can be carried out under milder conditions and in aqueous phase [30]. For instance, Lercher et al. reported that a combination of a metal (5 wt% Pd/C) catalyst and an acid (H_3PO_4) catalyst is efficient for HDO in aqueous medium [34]. The authors suggested that this catalytic route can be effectively applied for the HDO of diverse substituted phenolic monomers in upgrading bio-oil phenolic components. Such a strategy appears to be appropriate for the upgrading of the heavy fraction collected from our separation system.

There have been several recent reports in literature suggesting modifications of HDO catalysts that can lead to a more effective process for bio-oil upgrading with hydrogen. Such strategies are either based on solvents [31], or on the catalyst support [35–37]. Improvements have also been suggested by engineering the metal functionality in the catalysts by alloying the precious metal with a transition metal that leads to more reactive HDO catalysts [30]. A combination of different strategies such as upgrading of light components by C—C coupling reactions on mixed metal oxide, HDO of

Table 3
Component distribution from the control experiment with no catalyst bed.

Compound	In		Out					C accounted (%)
	wt%	mmol	Reactor drain[a] (mmol)	Separator drain		Gas phase (mmol)	Total (mmol)	
				Aqueous (mmol)	Organic (mmol)			
Acetic acid	20.0	209.7	198.2	2.5	0.0	0.0	200.7	95.7
Acetol	5.0	39.9	25.9	1.3	0.0	0.0	27.2	68.2
Furfural	10.0	71.6	52.3	0.6	2.4	13.5	68.9	96.2
p-Cresol	10.0	80.1	7.6	0.3	71.4	0.0	79.3	99.0
Levoglucosan	2.0	6.8	0.2	6.4	0.0	0.0	6.4	97.0
CO_2	0.0	0.0	0.0	0.0	0.0	3.0	3.0	–
CH_4	0.0	0.0	0.0	0.0	0.0	0.03	0.03	–
C_3H_8	0.0	0.0	0.0	0.0	0.0	0.21	0.21	–

[a] The reactor drain was obtained as a single liquid phase.

Table 4
Component distribution from catalytic conversion over $CeZrO_x$ catalyst bed.

Compound	In		Out						Conversion (%)
	wt%	mmol	Reactor drain		Separator drain		Gas phase (mmol)	Total (mmol)	
			Aqueous (mmol)	Organic (mmol)	Aqueous (mmol)	Organic (mmol)			
Acetic acid	20.0	234.7	59.2	23.8	3.5	3.5	0.0	90.0	61.6
Acetol	5.0	36.5	1.8	0.1	1.5	0.1	0.0	3.5	90.4
Furfural	10.0	79.6	11.9	27.9	0.7	3.8	12.0	56.3	29.2
p-Cresol	10.0	89.0	0.2	12.8	1.0	74.0	0.0	87.9	1.3
Levoglucosan	2.0	7.5	0.0	0.0	7.3	0.0	0.0	7.3	2.5
Acetone	–	–	14.1	7.7	0.0	0.0	47.5	69.3	–
CO_2	–	–	–	–	–	–	87.9	87.9	–
CO	–	–	–	–	–	–	9.3	9.3	–
HC (C1–C3)	–	–	–	–	–	–	0.3	0.3	–

phenolics, and in situ generation of hydrogen by aqueous phase reforming [38,39] would potentially be required in a bio-refinery for efficient upgrading of bio-oil to liquid transportation fuel.

3.6. Reaction mechanisms for acetol conversion

Our studies of bio-oil conversion indicate that it is possible to efficiently separate light and heavy ends of a simulated bio-oil, followed by upgrading the light end to obtain a low acid, low oxygen content intermediate oil that is appropriate for subsequent upgrading strategies, e.g., by C—C coupling reactions followed by hydro-deoxygenation under mild conditions to obtain liquid fuel grade components [21]. An important finding from the upgrading study was that $CeZrO_x$ not only converts the acetic acid but also efficiently convert most of the acetol to less reactive higher molecular weight compounds. The products from acetol mainly consisted of C_3–C_6 carbonyls.

To elucidate reaction mechanisms for acetol conversion over $CeZrO_x$, we carried out reaction kinetics studies with a feed of pure acetol (10 wt% in water) under similar reaction conditions as those used for bio-oil conversion (623 K, WHSV: 0.6 h^{-1}). The main products obtained were acetone, propanal, 2-butanone, 3-pentanone and 3-methylcyclopent-2-en-1-one, along with CO and CO_2. The carbon distribution of the product stream is presented in the first row of Table 5. It is evident that more than 70% of the carbon was retained as liquid products. Importantly, these liquid products are less reactive with lower oxygen content than the feed, which is a desirable outcome for bio-oil upgrading. This retention of liquid yield is not the case with other upgrading strategies such as hydrotreating, where carbon is lost as C_1–C_3 hydrocarbons [5].

To probe mechanisms for acetol conversion and to identify reaction intermediates, we increased the space velocity to 2.4 h^{-1}. At this higher space velocity, we observed an increase in the concentrations of acetic acid and propanal, indicating that these species are intermediate products from acetol. Secondly, we detected new products such as lactic acid and 2,5 hexanedione, which are also intermediates, suggesting that the overall reaction network consisted of several series and parallel reactions. Importantly, we also detected the presence of 1,2 propylene glycol. The formation of this species was not expected, because our reaction system does not employ an external source of hydrogen. To explain this observation, we propose that a transfer hydrogenation reaction (Scheme 2) is taking place over $CeZrO_x$, where two moles of acetol react to produce one mole each of pyruvaldehyde (dehydrogenated product) and 1,2-propylene glycol (hydrogenated product). In a recent study, Chia et al. reported that an array of metal oxides, including $CeZrO_x$, are efficient for catalytic transfer hydrogenation reactions [40]. It was noted that the amphoteric nature of the metal oxides is responsible for the effectiveness of the catalyst. $CeZrO_x$ mixed oxides possess both surface acid and base sites as confirmed by NH_3 and CO_2 TPD studies. This hypothesis also explains the formation of lactic acid (hydrolysis and rearrangement of pyruvaldehyde) and 2,5 hexanedione (cross aldol condensation of pyruvaldehyde with acetone, followed by hydrogenation). Moreover, the presence of saturated products suggested that there must also be an internal hydrogen source.

We calculated the thermochemistry of the hydrogen transfer step in Scheme 2 using Gaussian software. Fig. 4 indicates the Gibbs free energy and enthalpy (kJ/mol) for the transfer hydrogenation reaction, suggesting that the reaction is thermodynamically feasible. To further test our hypothesis, we carried out reaction kinetics measurements starting with pyruvaldehyde (10 wt% in water) and also with 1,2 propylene glycol (10 wt% in water) as feed. The reactions were performed at 623 K and a WHSV of 2.4 h^{-1}.

The product distribution from pyruvaldehyde is presented in the third row of Table 5. It can be seen that lactic acid is indeed one of the main products from pyruvaldehyde. Besides lactic acid, other main products from pyruvaldehyde include acetol, acetic

Table 5
Product distribution from the reaction of acetol and its transfer hydrogenation products over $CeZrO_x$ catalyst at 623 K.

Feed	WHSV (h^{-1})	Conversion (%)	C accounted (%)	Total C yield (%)					
Acetol	0.6	100	90.5	C1–C3 hydrocarbons:	0.1	*Light oxygenates:*	3.1	*C3–C6 oxygenates:*	61.3
				CO:	11.5	Acetaldehyde:	2.4	Propanal:	6.2
				CO_2:	14.6	Acetic acid:	0.7	Acetone:	26.4
								Acetoin:	1.8
								2-Butanone:	15.6
								3-Pentanone:	6.6
								3-Methyl-2-cycolpentenone:	4.7
Acetol	2.4	74.2	81.1	C1–C3 hydrocarbons	0.1	*Light oxygenates:*	10.8	*C3–C6 oxygenates:*	37.6
				CO:	3.8	Acetaldehyde:	3.4	Lactic acid	0.7
				CO_2:	3.2	Acetic acid:	7.3	Acetone	16.7
						Ethanol:	0.1	Propanal:	5.3
								Acetoin:	2.2
								1,2-Propylene glycol:	2.7
								2-Butanone:	4.1
								3-Pentanone:	1.5
								2,5-hexanedione:	2.3
								3-Methyl-2-cycolpentenone:	2.1
Pyruvaldehyde	2.4	60.1	91.6	C1–C3 hydrocarbons	0.2	*Light oxygenates:*	17.2	*C3–C6 oxygenates:*	27.8
				CO:	2.9	Formaldehyde:	3.6	Acetol:	17.7
				CO_2:	3.6	Acetaldehyde:	4.8	Propanal:	0.3
						Acetic acid:	8.8	Acetone:	0.5
								Lactic acid	7.8
								1,2-propylene glycol:	0.5
								2-butanone:	0.8
								2,5-Hexanedione:	0.2
1,2 Propylene glycol	2.4	77.3	82.2	C1–C3 hydrocarbons	0.3	*Light oxygenates:*	6.1	*C3–C6 oxygenates:*	46.7
				CO:	3.3	Acetaldehyde:	1.9	Propanal:	5.9
				CO_2:	3.1	Acetic acid:	0.7	Acetol:	1.4
						Ethanol:	3.5	Acetone:	13.4
								Allyl Alcohol:	5.5
								Propanol:	9.4
								2-Butanone:	6.2
								3-Pentanone:	2.3
								2,5-Hexanedione:	0.2
								3-Methyl-2-cycolpentenone:	2.4

acid, formaldehyde, acetaldehyde and acetone, along with CO and CO_2. Based on this product distribution, we propose a reaction scheme (Fig. 4), where pyruvaldehyde (**1**) undergoes α-dicarbonyl cleavage [41–43] on the basic sites on the $CeZrO_x$ in the presence of water to produce a mole each of acetic acid (**1A**) and formaldehyde (**1B**), or a mole of formic acid (**1C**) and acetaldehyde (**1D**) as primary products. Acetic acid formed as a primary product from pyruvaldehyde undergoes ketonization to form acetone (**1E**) as a secondary product, along with the production of CO_2 and H_2O. Acetic acid also undergoes ketonization with lactic acid (**1F**) to form 3-hydroxybutanone (acetoin, **1G**). Formaldehyde and formic acid produced in the primary step can subsequently serve as reducing agents in the overall reaction scheme to produce the observed hydrogenated products. In addition, formaldehyde and formic acid can undergo decomposition to produce CO and CO_2, respectively, along with H_2 in each case, which serves as an internal source of hydrogen for the hydrogenation reactions. The production of H_2 by formic acid dehydrogenation over zirconia among other metal oxides is well known in the literature [44], and this H_2 can adsorb on the metal oxide surface [45,46] to perform hydrogenation reactions, yielding saturated products [47,48]. We performed stoichiometric calculations which indicated that the amount of hydrogen produced was sufficient to carry out the hydrogenation reactions observed.

The acetone produced as a secondary product also undergoes aldol condensation with pyruvaldehyde, followed by hydrogenation to form 2,5 hexanedione (**1H**), which undergoes an intra-molecular aldol condensation to form 3-methylcyclopent-2-en-1-one (**1I**). Thus, the formation of acetone, acetoin and 3-methylcyclopent-2-en-1-one can be explained as occurring via the initial formation of pyruvaldehyde. Other C_5–C_6 ketones observed as minor products were formed as a result of condensation reactions, some followed by ring closure.

The product distribution from 1,2-propylene glycol (**2**), the hydrogenated product of the transfer hydrogenation reaction in Scheme 2, is presented in the last row of Table 5. Based on the observed products, we propose that the primary products from 1,2-propylene glycol result from dehydration reactions on the surface acid sites, leading to allyl alcohol (**2A**), propanal (**2B**) and acetone (**2C**) [49]. Dehydrogenation of 1,2-propylene glycol leads to the

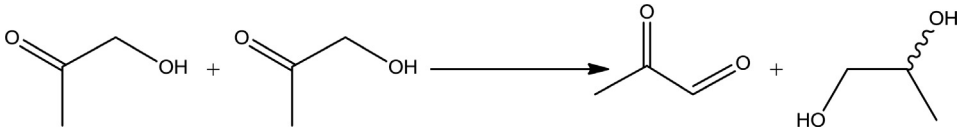

Scheme 2.

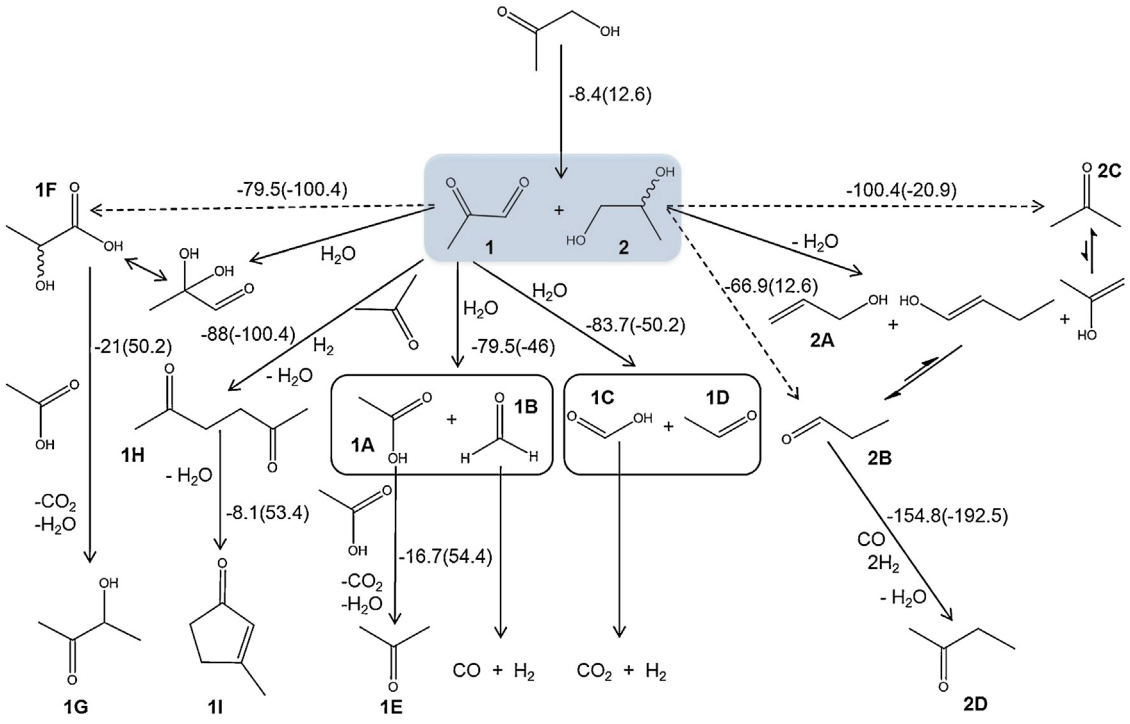

Fig. 4. Reaction network and thermodynamics involved in the conversion of acetol over $CeZrO_x$ catalyst at 623 K. Values outside the parentheses correspond to ΔG° (kJ/mol) and inside the parenthesis correspond to ΔH° (kJ/mol).

formation of acetol [50]. Propanal produced in the primary step undergoes reaction to form 2-butanone (**2D**) [7,51]. Propanal also undergoes disproportionation to form propionic acid and propanol, which was also observed as an intermediate product. Propionic acid undergoes ketonization to form 3-pentanone. Thus, the formation of propanal, acetone, 2-butanone and 3-pentanone can be explained as occurring via the initial formation of 1,2-propylene glycol.

The results from reaction kinetics measurements for conversion of pyruvaldehyde and 1,2-propylene glycol are thus consistent with reaction kinetics measurements for conversion of acetol, indicating the importance of transfer hydrogenation products over the $CeZrO_x$ mixed oxide catalyst. The entire reaction network suggested from this work is presented in Fig. 4, along with the thermochemical quantities (Gibbs free energy and Enthalpy of reaction (kJ/mol)) for various reactions involved. The primary reaction in the conversion of acetol is a transfer hydrogenation reaction producing pyruvaldehyde and 1,2 propylene glycol. These two primary products then undergo reactions in series and parallel to produce an array of C_3–C_6 carbonyl compounds, constituting an upgraded intermediate feed appropriate for further processing steps.

4. Conclusions

We present a catalytic strategy for the conversion of the light fraction of a simulated bio-oil over a $CeZrO_x$ mixed oxide catalyst. While the simulated bio-oil is significantly simplified relative to real bio-oil, the simulated bio-oil contained representative molecules of the key functional group classes present in real bio-oil. The $CeZrO_x$ catalyst resulted in selective ketonization of acetic acid in the presence of furfural and acetol. The presence of furfural caused the reversible suppression of ketonization activity. Acetol was highly reactive over the mixed oxide, and its presence did not influence the ketonization activity. Reaction kinetics studies revealed that the primary step in the conversion of acetol is a transfer hydrogenation reaction producing pyruvaldehyde and 1,2 propylene glycol. Subsequently, ketones in C_3–C_6 range are produced as a result of reactions in series and parallel occurring over $CeZrO_x$ catalyst. The results from this study provide a fundamental understanding of the reactions taking place during catalytic upgrading of the aqueous fraction of bio-oil over a mixed oxide catalyst. This strategy not only converts the acid content of bio-oil, but it retains most of the carbon from reactive acetol in the form of liquid products that are less reactive, have higher molecular weight, and have lower oxygen content. This approach thus produces an intermediate feed that is appropriate for further upgrading to obtain transportation fuel grade components.

Acknowledgement

We acknowledge financial support from the Department of Energy for this work.

References

[1] G.W. Huber, A. Corma, Angewandte Chemie: International Edition English 46 (2007) 7184–7201.
[2] G.W. Huber, S. Iborra, A. Corma, Chemical Reviews (Washington, DC, US) 106 (2006) 4044–4098.
[3] T.P. Vispute, G.W. Huber, Green Chemistry 11 (2009) 1433–1445.
[4] D.M. Alonso, J.Q. Bond, J.A. Dumesic, Green Chemistry 12 (2010) 1493–1513.
[5] D.E. Resasco, Journal of Physical Chemistry Letters 2 (2011) 2294–2295.
[6] C.A. Gärtner, J.C. Serrano-Ruiz, D.J. Braden, J.A. Dumesic, Journal of Catalysis 266 (2009) 71–78.
[7] A. Gangadharan, M. Shen, T. Sooknoi, D.E. Resasco, R.G. Mallinson, Applied Catalysis A 385 (2010) 80–91.
[8] E.I. Gurbuz, E.L. Kunkes, J.A. Dumesic, Green Chemistry 12 (2010) 223–227.
[9] M. Renz, European Journal of Organic Chemistry 6 (2005) 979–988.
[10] Y. Yamada, M. Segawa, F. Sato, T. Kojima, S. Sato, Journal of Molecular Catalysis A: Chemical 346 (2011) 79–86.
[11] O. Nagashima, S. Sato, R. Takahashi, T. Sodesawa, Journal of Molecular Catalysis A: Chemical 227 (2005) 231–239.
[12] L. Deng, Y. Fu, Q.-X. Guo, Energy and Fuels 23 (2009) 564–568.
[13] A.S. Pollard, M.R. Rover, R.C. Brown, Journal of Analytical and Applied Pyrolysis 93 (2012) 129–138.
[14] M.A. Hasan, M.I. Zaki, L. Pasupulety, Applied Catalysis A 243 (2003) 81–92.
[15] R.W. Snell, B.H. Shanks, Applied Catalysis A 451 (2013) 86–93.

[16] T.N. Pham, D. Shi, T. Sooknoi, D.E. Resasco, Journal of Catalysis 295 (2012) 169–178.
[17] J.I. Gutiérrez-Ortiz, B. de Rivas, R. López-Fonseca, J.R. González-Velasco, Journal of Thermal Analysis and Calorimetry 80 (2005) 225–228.
[18] H. Vidal, J. Kaspar, M. Pijolat, G. Colon, S. Bernal, A. Cordon, V. Perrichon, F. Fally, Applied Catalysis B 27 (2000) 49–63.
[19] J.C. Serrano-Ruiz, J. Luettich, A. Sepúlveda-Escribano, F. Rodríguez-Reinoso, Journal of Catalysis 241 (2006) 45–55.
[20] J. Di Cosimo, Journal of Catalysis 208 (2002) 114–123.
[21] E.L. Kunkes, D.A. Simonetti, R.M. West, J.C. Serrano-Ruiz, C.A. Gartner, J.A. Dumesic, Science 322 (2008) 417–421.
[22] K.S.W. Sing, Pure and Applied Chemistry 54 (1985) 2201–2218.
[23] E.I. Gurbuz, E.L. Kunkes, J.A. Dumesic, Applied Catalysis B 94 (2010) 134–141.
[24] R.M. West, Z.Y. Liu, M. Peter, C.A. Gaertner, J.A. Dumesic, Journal of Molecular Catalysis A: Chemical 296 (2008) 18–27.
[25] H. Kawamoto, S. Saito, S. Saka, Journal of Analytical and Applied Pyrolysis 82 (2008) 78–82.
[26] T. Hosoya, H. Kawamoto, S. Saka, Carbohydrate Research 341 (2006) 2293–2297.
[27] D.C. Elliott, T.R. Hart, G.G. Neuenschwander, L.J. Rotness, A.H. Zacher, Environmental Progress & Sustainable Energy 28 (2009) 441–449.
[28] D.C. Elliott, T.R. Hart, Energy and Fuels 23 (2009) 631–637.
[29] T.V. Choudhary, C.B. Phillips, Applied Catalysis A 397 (2011) 1–12.
[30] P.T.M. Do, A.J. Foster, J. Chen, R.F. Lobo, Green Chemistry 14 (2012) 1388.
[31] H. Wan, R.V. Chaudhari, B. Subramaniam, Topics in Catalysis 55 (2012) 129–139.
[32] D.C. Elliott, Energy and Fuels 21 (2007) 1792–1815.
[33] E. Laurent, B. Delmon, Journal of Catalysis 146 (1994) 281–291.
[34] C. Zhao, Y. Kou, A.A. Lemonidou, X. Li, J.A. Lercher, Angewandte Chemie: International Edition English 48 (2009) 3987–3990.
[35] A. Centeno, E. Laurent, B. Delmon, Journal of Catalysis 154 (1995) 288–298.
[36] D.-Y. Hong, S.J. Miller, P.K. Agrawal, C.W. Jones, Chemical Communications (Cambridge, UK) 46 (2010) 1038.
[37] T. Nimmanwudipong, C. Aydin, J. Lu, R.C. Runnebaum, K.C. Brodwater, N.D. Browning, D.E. Block, B.C. Gates, Catalysis Letters 142 (2012) 1190–1196.
[38] R.D. Cortright, R.R. Davda, J.A. Dumesic, Nature (London, UK) 418 (2002) 964–967.
[39] J. Fu, S.H. Hakim, B.H. Shanks, Topics in Catalysis 55 (2012) 140–147.
[40] M. Chia, J.A. Dumesic, Chemical Communications (Cambridge, UK) 47 (2011) 12233–12235.
[41] J.M. Debruijn, A.P.G. Kieboom, H. Vanbekkum, Starch-Starke 39 (1987) 23–28.
[42] A.V. Ellis, M.A. Wilson, Journal of Organic Chemistry 67 (2002) 8469–8474.
[43] Z. Srokol, A.-G. Bouche, A. van Estrik, R.C.J. Strik, T. Maschmeyer, J.A. Peters, Carbohydrate Research 339 (2004) 1717–1726.
[44] P.A. Dilara, J.M. Vohs, Journal of Physical Chemistry 97 (1993) 12919–12923.
[45] J. Kondo, Y. Sakata, K. Domen, K. Maruya, T. Onishi, Journal of Chemical Society Faraday Transactions 86 (1990) 397.
[46] H. Nakatsuji, M. Hada, H. Ogawa, K. Nagata, K. Domen, Journal of Physical Chemistry 98 (1994) 11840–11845.
[47] A. Sofianos, Catalysis Today 15 (1992) 149–175.
[48] Z. Feng, Journal of Catalysis 148 (1994) 84–90.
[49] K. Mori, Y. Yamada, S. Sato, Applied Catalysis A 366 (2009) 304–308.
[50] Z. Yu, L. Xu, X. Zhang, Z. Liu, Chinese Journal of Catalysis 31 (2010) 441–446.
[51] L. Lietti, E. Tronconi, P. Forzatti, Journal of Catalysis 135 (1992) 400–419.